International Journal of
Mathematics And its Applications
ISSN: 2347-1557

Int. J. Math. And Appl., **14(2)**(2026), 91–116
Available Online: http://ijmaa.in

Effect of Chemical Reaction on Heat and Mass Transfer in MHD Rotating Flow of a Couple Stress Fluid through a Porous Medium with Temporal Oscillatory Permeability

Mithilesh Kumar Mishra[1,*], Anjali Kumari[2], Richa Tripathi[2], Deepak Kumar[1], Atul Kumar[3]

[1]*Department of Mathematics, L.N.D.College Motihari (A Constituent Unit of Babasaheb Bhimrao Ambedkar Bihar University, Muzaffarpur), Bihar, India*

[2]*Department of Mathematics, Gaya College, Gaya Ji (A Constituent Unit of Magadh University, Bodh gaya), Bihar, India*

[3]*Department of Mathematics, Applied Science and Humanities Government Engineering College, Samastipur (A Constituent Unit of Bihar Engineering University, Patna), Bihar, India*

Abstract

The present investigation focuses on the analysis of heat and mass transfer characteristics in an unsteady free convective magnetohydrodynamic (MHD) rotating flow of a couple-stress fluid past a vertical porous plate embedded in a porous medium. The study incorporates the effects of time-dependent oscillatory suction and permeability, along with the presence of an internal heat generation source and a first-order homogeneous chemical reaction. The influence of an externally applied transverse magnetic field is also taken into account to examine its role in controlling the flow dynamics. The governing system of highly nonlinear partial differential equations describing the conservation of momentum, energy, and species concentration is formulated under appropriate physical assumptions. These equations are rendered dimensionless using suitable similarity transformations and are subsequently decomposed into steady and oscillatory components to facilitate analytical treatment. The resulting coupled nonlinear differential equations are solved numerically using an efficient numerical scheme. A comprehensive parametric study is carried out to illustrate the effects of key dimensionless parameters, such as the magnetic field parameter, rotation parameter, couple-stress parameter, permeability parameter, heat source parameter, and chemical reaction parameter, on the velocity, temperature, and concentration distributions. The numerical results are presented graphically and discussed in detail to highlight the underlying physical mechanisms governing the flow behaviour. The findings of this study are expected to be useful in understanding complex transport phenomena in engineering and industrial processes involving non-Newtonian fluids, porous media, and MHD applications.

Keywords: MHD Flow; Mass and heat transfer; Chemical Reaction; Porous Medium; Non linear PDE.

2020 Mathematics Subject Classification: 76E25, 76S05, 80A19, 80A32, 35M86.

*Corresponding author (mithileshmishra0194@gmail.com)

Nomenclature

C	Species concentration	σ	Electrical conductivity
D	Molecular diffusivity	ω^*	Non-dimensional frequency of oscillation
K_p	Permeability of the medium	ϕ	Non-dimensional Couple Stress Parameters
α	Thermal diffusivity	G_c	Grashof number for mass transfer
η	Couple stress parameter	g	Acceleration due to gravity
E	Rotation parameter	K	Porosity parameter
N_u	Nusselt number	M	Magnetic parameter
S	Heat source parameter	B_0	Magnetic field of uniform strength
S_h	Sherwood number	P_r	Prandtl number
T^*	Non-dimensional temperature	S_c	Schmidt number
T	Temperature of the fluid	t'	time
u	Non-dimensional velocity	u'	Velocity component along x-axis
w_0	Constant suction velocity	$w(t')$	Suction velocity
y	Non-dimensional distance along y-axis	y'	Distance along y-axis
ε	A Small positive constant	ρ	Density of the Fluid
β	Volumetric coefficient of expansion for heat transfer	β^*	Volumetric coefficient of expansion with species concentration
$\frac{\mu}{\rho}$	Kinematic coefficient of viscosity	ω	Frequency of oscillation
τ	Skin friction	G_r	Grashof number for heat transfer
w	Condition on porous plate	μ	Viscosity
P	Pressure gradient	t^*	Non dimensional time
C^*	Non dimensional Species Concentration	K_c	Chemical reaction parameter

1. Introduction

In recent years, the study of magnetohydrodynamic (MHD) rotating flow of couple-stress fluids through porous media has gained significant attention due to its extensive applications in geophysical, industrial, and engineering processes. The couple-stress fluid model incorporates micro-rotational effects and particle-size influences, thereby providing a more realistic representation of complex fluids such as biological fluids, lubricants, and polymeric suspensions than conventional Newtonian models. The interaction of such fluids with a porous medium in the presence of an applied transverse magnetic field gives rise to a complex interplay among viscous forces, couple-stress effects, magnetic forces, and porous resistance, which substantially alters the momentum transport characteristics. Furthermore, chemical reactions modify the concentration distribution, thereby affecting buoyancy-induced flow behavior and mass transfer rates. An in-depth understanding of these coupled effects is essential for the optimal design and analysis of chemical

reactors, filtration systems, and biomedical devices involving electrically conducting fluids.

The study of magnetohydrodynamic (MHD) rotating flow accompanied by coupled heat and mass transfer through porous media has garnered considerable research attention due to its wide-ranging applications in geothermal energy extraction, enhanced oil recovery, chemical processing operations, thermal insulation systems, and cooling technologies. Initial investigations in this area primarily concentrated on analyzing the effects of porous media properties and applied magnetic fields on convective heat and mass transfer phenomena.

Das *et al.* [1] examined mass transfer effects on MHD flow past a vertical porous plate under oscillatory suction and internal heat generation, demonstrating the strong control of suction on velocity, temperature, and concentration profiles. Bhargava *et al.* [2] extended this analysis by incorporating chemical reaction along with Soret and Dufour effects using finite element modeling techniques. The effects of unsteady flow and viscoelastic behavior were later incorporated into MHD porous media studies. Kumar and Satyanarayana [3] analyzed unsteady MHD free convective Walter's memory flow with constant suction and heat sink, while Ravikumar *et al.* [4] investigated heat and mass transfer in viscous fluid flow through a non-homogeneous porous medium with temperature-dependent heat source.

Hussaini *et al.* [5] further studied unsteady memory convective flow under variable suction conditions, highlighting the sensitivity of flow dynamics to suction velocity. Considerable attention has been devoted to viscoelastic and non-Newtonian fluid models. Mishra *et al.* [6] studied mass and heat transfer effects on MHD flow of a viscoelastic fluid through a porous medium with oscillatory suction and heat source.

Rahman *et al.* [7] performed numerical investigations on chemically reacting MHD flow with Soret and Dufour effects in a rotating system. Mohanty *et al.* [8] analyzed MHD viscoelastic fluid flow through a non-homogeneous porous medium, considering oscillatory suction and heat source/sink effects. Radiative heat transfer and chemical reaction effects were included by Seth *et al.* [9], who examined unsteady MHD natural convection flow of a chemically reactive and radiating fluid past a moving vertical porous plate.

Ali *et al.* [10] investigated MHD flow and heat transfer of couple stress fluids over oscillatory stretching sheets embedded in porous media. Umamaheswar *et al.* [11] analyzed MHD double-diffusive chemically reactive flow through a rotating porous plate, while Singh *et al.* [12] studied Hall and ion-slip effects on oscillatory MHD flow of a rotating fluid. Further developments include the study of micropolar and radiating fluids in porous media. Pal and Biswas [13] examined oscillatory MHD convective-radiative flow of a chemically reactive micropolar fluid in a porous medium. Emeka *et al.* [14] investigated free convection boundary layer flow of a rotating MHD fluid past a vertical porous medium under thermal radiation.

Krishna and Chamkha [15] analyzed MHD peristaltic rotating flow of a couple stress fluid through a porous medium, incorporating wall slip effects. Recent studies have emphasized rotating porous

systems and advanced physical effects. Das and Das [16] examined unsteady MHD rotating chemically reacting flow over an oscillating vertical surface in a Darcian porous regime. Bafakeeh *et al.* [17] studied Hall current and Soret effects on unsteady MHD rotating flow of second-grade fluids under thermal radiation and chemical reaction influences. Naveed *et al.* [18] analyzed heat transfer in hydromagnetic couple stress fluid flow with homogeneous and heterogeneous chemical reactions over a porous oscillatory stretching sheet. Very recent investigations have focused on hybrid nanofluids, rotating porous channels, and slip effects.

Mahesh *et al.* [19] examined radiation effects on MHD couple stress hybrid nanofluid flow over a porous sheet with viscous dissipation. Sharma *et al.* [20] presented a mathematical analysis of chemically reacting MHD free convection flow through a rotating porous medium with radiation effects. Verma and Ansari [21,22] investigated Darcy–Brinkman flow in an anisotropic rotating porous channel under magnetic field influence and later extended their work to include viscous dissipation and slip boundary conditions.

The present study aims to examine the effects of variable permeability and oscillatory suction velocity on the convective mass transfer characteristics of a rotating couple-stress fluid flowing past an infinite vertical porous plate embedded in a porous medium. The analysis is carried out in the presence of a uniform transverse magnetic field and a chemical reaction. The findings of this study are expected to be useful in understanding and improving various practical processes, including groundwater flow systems, geothermal energy applications, the transport of chemical fertilizers in soil, and oil extraction operations.

2. Mathematical Formulation

An unsteady free convective rotating flow of a couple-stress fluid past an infinite vertical porous plate embedded in a porous medium is considered in the presence of a transverse magnetic field. The permeability of the porous medium as well as the suction velocity at the plate are assumed to vary harmonically with time. The coordinate system is chosen such that the x-axis is aligned with the vertical plate in the direction of flow, while the y-axis is normal to it.

Since the magnetic Reynolds number is assumed to be sufficiently small (less than unity), the induced magnetic field is neglected compared to the applied magnetic field. Consequently, the flow is governed primarily by buoyancy forces arising from temperature and concentration gradients.Initially ($t = 0$), the plate and the fluid are at the same temperature and species concentration, and the Soret and Dufour effects are neglected. For $t > 0$, the plate temperature and concentration are instantaneously raised to constant values T_w and C_w, respectively.The physical configuration of the problem is illustrated in Fig. 1.

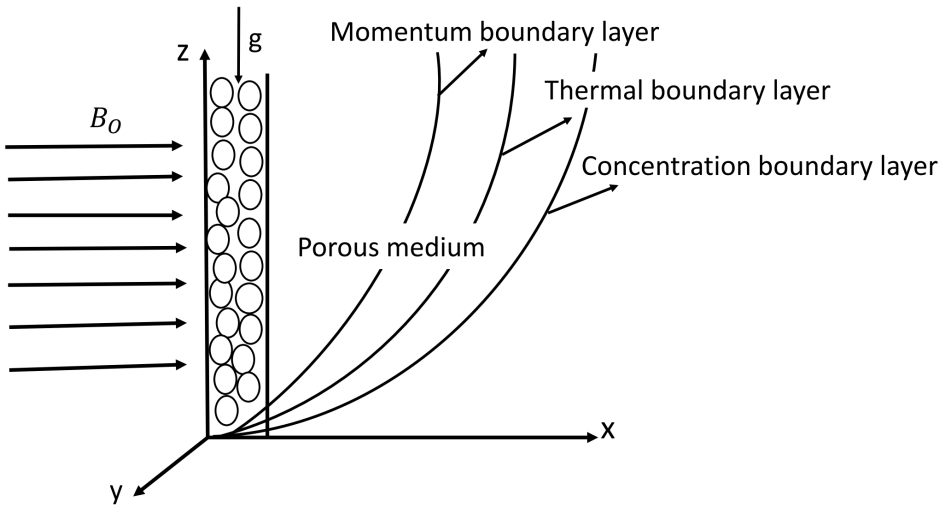

Figure 1: The physical configuration of the system under consideration.

The time-dependent oscillatory permeability of the porous medium and the suction velocity are assumed to be of the following form

$$K(t') = K_p\left(1 + \epsilon e^{i\omega t}\right) \tag{1}$$

$$w(t') = -w_0\left(1 + \epsilon e^{i\omega t}\right) \tag{2}$$

Here, $w_0 > 0$ and $\epsilon \ll 1$ are positive constants. Under the above assumptions and the conventional Boussinesq approximation, the governing equations in the rotating frame of reference are given by

$$\frac{\partial u'}{\partial t'} + w\frac{\partial u'}{\partial z'} - 2\Omega v = -\frac{1}{\rho}\frac{\partial P}{\partial x'} + \frac{\mu}{\rho}\frac{\partial^2 u'}{\partial z'^2} + g\beta(T - T_\infty) + g\beta^*(C - C_\infty) - \frac{\sigma B_0^2 u'}{\rho} - \frac{\mu u'}{K_p\rho(1 + \epsilon e^{i\omega t})} - \frac{\eta}{\rho}\frac{\partial^4 u'}{\partial z'^4} \tag{3}$$

$$\frac{\partial v'}{\partial t'} + w\frac{\partial v'}{\partial z'} + 2\Omega u = -\frac{1}{\rho}\frac{\partial P}{\partial y'} + \frac{\mu}{\rho}\frac{\partial^2 v'}{\partial z'^2} - \frac{\sigma B_0^2 v'}{\rho} - \frac{\mu v'}{K_p\rho(1 + \epsilon e^{i\omega t})} - \frac{\eta}{\rho}\frac{\partial^4 v'}{\partial z'^4} \tag{4}$$

$$\frac{\partial T}{\partial t'} + w\frac{\partial T}{\partial z'} = \alpha\frac{\partial^2 T}{\partial z'^2} + S'(T - T_\infty) \tag{5}$$

$$\frac{\partial C}{\partial t'} + w\frac{\partial C}{\partial z'} = D\frac{\partial^2 C}{\partial z'^2} - K_c'(C - C_\infty) \tag{6}$$

The Boundary conditions are

$$\left.\begin{aligned} &u' = 0, \quad T = T_w + \epsilon(T_w - T_\infty)e^{i\omega t}, \quad C = C_w + \epsilon(C_w - C_\infty)e^{i\omega t}, \quad \frac{\partial^2 u'}{\partial z'^2} = 0 \quad \text{at } z = 0 \\ &u' \to 0, \quad T \to T_\infty, \quad C \to C_\infty, \quad \frac{\partial^2 u'}{\partial z'^2} \to 0 \quad \text{as } z \to \infty \end{aligned}\right\} \tag{7}$$

Combining (3) and (4) we obtain, let $q = u' + iv'$ and $\xi = x' - iy'$

$$\frac{\partial q}{\partial t'} + w\frac{\partial q}{\partial z'} + 2i\Omega q = -\frac{1}{\rho}\frac{\partial p}{\partial \xi} + \frac{\mu}{\rho}\frac{\partial^2 q}{\partial z'^2} + g\beta(T - T_\infty) + g\beta^*(C - C_\infty)$$

$$-\frac{\sigma B_0^2 q}{\rho}-\frac{\mu q}{K_p\rho(1+\varepsilon e^{i\omega t})}-\frac{\eta}{\rho}\frac{\partial^4 q}{\partial z'^4} \tag{8}$$

Equation (2) governs the dynamics of the complex velocity q by accounting for temporal variation and axial convection, along with the Coriolis force induced by system rotation, balanced against the pressure gradient, viscous diffusion, buoyancy forces arising from thermal and concentration gradients, the magnetic Lorentz force, resistance due to oscillatory permeability of the porous medium, and a higher-order diffusion term representing couple-stress effects. For the boundary-layer formulation, the dynamic viscosity μ and the couple-stress parameter η are considered to be of comparable order, thereby ensuring that viscous and couple-stress effects jointly and significantly influence the flow characteristics.

3. Non - Dimensionalization of Flow Quantities

To nondimensionalize the governing equations and the associated boundary conditions of the flow, the following dimensionless variables and parameters are introduced.

$$\left.\begin{array}{l} z^*=\dfrac{w_0 z'\rho}{\mu},\quad t^*=\dfrac{w_0^2 t'\rho}{4\mu},\quad \omega^*=\dfrac{4\mu\omega}{w_0^2\rho},\quad q^*=\dfrac{q}{w_0},\quad T^*=\dfrac{T-T_\infty}{T_w-T_\infty},\quad C^*=\dfrac{C-C_\infty}{C_w-C_\infty} \\ P=\dfrac{\partial P}{\partial\xi},\quad S=\dfrac{\mu S'}{\rho w_0^2},\quad \phi=\dfrac{\eta w_0^2\rho^2}{\mu^3},\quad E=\dfrac{\Omega\mu}{w_0^2\rho},\quad K=\dfrac{w_0^2 K_p\rho^2}{\mu^2},\quad P_r=\dfrac{\mu}{\alpha\rho},\quad S_c=\dfrac{\mu}{\rho D} \\ M^2=\dfrac{\sigma B_0^2\mu}{w_0^2\rho^2},\quad G_r=\dfrac{\mu g\beta(T_w-T_\infty)}{\rho w_0^3},\quad G_c=\dfrac{\mu g\beta^*(C_w-C_\infty)}{\rho w_0^3},\quad \mathrm{K}_c=\dfrac{\mu K_c'}{\rho u_0^2} \end{array}\right\} \tag{9}$$

By employing the non-dimensional parameters introduced in equation (9) and applying them to Equations (1) and (2), the governing flow equations along with the boundary conditions 3 to 7 are transformed into the following non-dimensional form:

$$\left.\frac{1}{4}\frac{\partial q}{\partial t}-\left(1+\epsilon e^{i\omega t}\right)\frac{\partial q}{\partial z}+2iEq=-\frac{\mu P}{w_0^3\rho^2}+\frac{\partial^2 q}{\partial z^2}+G_r T+G_c C-M^2 q-\frac{q}{K(1+\epsilon e^{i\omega t})}-\phi\frac{\partial^4 q}{\partial z^4}\right\} \tag{10}$$

$$\left.\frac{1}{4}\frac{\partial T}{\partial t}-\left(1+\epsilon e^{i\omega t}\right)\frac{\partial T}{\partial z}=\frac{1}{P_r}\frac{\partial^2 T}{\partial z^2}+ST\right\} \tag{11}$$

$$\left.\frac{1}{4}\frac{\partial C}{\partial t}-\left(1+\epsilon e^{i\omega t}\right)\frac{\partial C}{\partial z}=\frac{1}{S_c}\frac{\partial^2 C}{\partial z^2}-K_c C\right\} \tag{12}$$

Boundary Conditions are -

$$\left.\begin{array}{lll} q=0,\quad T=1+\epsilon e^{i\omega t},\quad C=1+\epsilon e^{i\omega t}, & \dfrac{\partial^2 q}{\partial z^2}=0,\quad \text{at } z=0 \\ q\to 0,\quad T\to 0,\quad C\to 0, & \dfrac{\partial^2 q}{\partial z^2}\to 0,\quad \text{as } z\to\infty \end{array}\right\} \tag{13}$$

4. Method of Solution

Taking into consideration the effects of periodic suction and the temperature and concentration variations in the vicinity of the plate, the velocity, temperature, and concentration fields near the plate are assumed to be of the following form:

$$q(z,t) = u_0(z) + \varepsilon u_1(z)e^{i\omega t} \tag{14}$$

$$T(z,t) = T_0(z) + \varepsilon T_1(z)e^{i\omega t} \tag{15}$$

$$C(z,t) = C_0(z) + \varepsilon C_1(z)e^{i\omega t} \tag{16}$$

The above solution methodology has been employed by Mishra *et al.* [10], Das *et al.* [3], and Gireesh Kumar and Satyanarayana [4] to analyze periodically fluctuating flow problems. By substituting Equations 14 to 16 into Equations 10 to 12 and equating the coefficients of the non-harmonic terms (of order ϵ^0) and harmonic terms (of order ϵ), the resulting governing equations are obtained as follows:

$$-\phi\frac{d^4u_0}{dz^4} + \frac{d^2u_0}{dz^2} + \frac{du_0}{dz} - \left(M^2 + 2iE + \frac{1}{K}\right)u_0 = -G_rT_0 - G_cC_0 - \frac{\mu P}{w_0^3\rho^2} \tag{17}$$

$$-\phi\frac{d^4u_1}{dz^4} + \frac{d^2u_1}{dz^2} - \left(M^2 + 2iE + \frac{1}{K} + \frac{i\omega}{4}\right)u_1 = -\frac{du_0}{dz} - G_rT_1 - G_cC_1 - \frac{u_0}{K} \tag{18}$$

$$\frac{d^2T_0}{dz^2} + P_r\frac{dT_0}{dz} + P_rST_0 = 0 \tag{19}$$

$$\frac{d^2T_1}{dz^2} + P_r\frac{dT_1}{dz} + P_r(S - \frac{i\omega}{4})T_1 = -P_r\frac{dT_0}{dz} \tag{20}$$

$$\frac{d^2C_0}{dz^2} + S_c\frac{dC_0}{dz} - K_cS_cC_0 = 0 \tag{21}$$

$$\frac{d^2C_1}{dz^2} + S_c\frac{dC_1}{dz} - \frac{i\omega}{4}S_cC_1 - K_cS_cC_1 = -S_c\frac{dC_0}{dz} \tag{22}$$

The boundary conditions now reduce to

$$\left.\begin{aligned} u_0 = u_1 = 0, \quad T_0 = T_1 = 1, \quad C_0 = C_1 = 1 \quad & \text{at } z = 0, \\ u_0 = u_1 \to 0, \quad T_0 = T_1 \to 0, \quad C_0 = C_1 \to 0 \quad & \text{as } z \to \infty, \\ \frac{d^2u_0}{dz^2} = 0 \quad \& \quad \frac{d^2u_1}{dz^2} = 0 \quad & \text{at } z = 0, \\ \frac{d^2u_0}{dz^2} \to 0 \quad \& \quad \frac{d^2u_1}{dz^2} \to 0 \quad & \text{as } z \to \infty. \end{aligned}\right\} \tag{23}$$

The differential equations 17 to 22 , along with the associated boundary conditions 23, describing the velocity $q(z,t)$, temperature $T(z,t)$, and concentration $C(z,t)$, are solved numerically by employing the fourth-order Runge–Kutta method.

4.1 Skin-friction Coefficient (τ)

The shear stress (skin friction) at the plate, expressed in terms of its amplitude, is defined as follows.

$$\tau = \left.\frac{\partial u_0}{\partial z}\right|_{z=0} + \varepsilon e^{i\omega t} \left.\frac{\partial u_1}{\partial z}\right|_{z=0} - \phi \left[\left.\frac{\partial^3 u_0}{\partial z^3}\right|_{z=0} + \varepsilon e^{i\omega t} \left.\frac{\partial^3 u_1}{\partial z^3}\right|_{z=0} \right]$$

4.2 Nusselt Number (N_u)

The rate of heat transfer (heat flux) at the plate, represented in terms of its amplitude, is given by the following expression.

$$N_u = - \left[\left.\frac{\partial T_0}{\partial z}\right|_{z=0} + \varepsilon e^{i\omega t} \left.\frac{\partial T_1}{\partial z}\right|_{z=0} \right]$$

4.3 Sherwood Number (S_h)

The mass transfer coefficient (Sherwood number) at the plate, formulated in terms of its amplitude, is expressed as follows.

$$S_h = - \left[\left.\frac{\partial C_0}{\partial z}\right|_{z=0} + \varepsilon e^{i\omega t} \left.\frac{\partial C_1}{\partial z}\right|_{z=0} \right]$$

5. Results and Discussion

Magnetohydrodynamic (MHD) flows of non-Newtonian fluids through porous media have attracted considerable attention due to their significant applications in engineering and industrial processes such as polymer processing, geothermal energy extraction, and biomedical systems. In particular, couple stress fluids provide a more realistic model for fluids with microstructure, where the effects of particle size and micro-rotational interactions become important.

The flow scenario is illustrated in Figure 1. It depicts convective flow of an incompressible, electrically conducting Rotating couple-stress fluid past a vertical porous plate within a porous medium with chemical reaction, and time-dependent oscillatory permeability and suction. The flow is influenced by the non-dimensional parameters Hartmann number M, Permeability Parameter K_p, Thermal Grashof number G_r, Mass Grashof number G_c, Frequency of oscillation ω, Schmidt number S_c, Prandtl number P_r, Heat source parameter S, Couple Stress parameter ϕ, Rotation parameter E, Constant suction w_0 , Chemical reaction parameter K_c.

The results of the numerical evaluation for various values of the governing parameters are shown graphically in Figures 2 to 11 and Tables 1 to 18. In the numerical work, We take $M = 2$, $\omega = 1$, $\phi = 2$, $K = 0.6$, $P_r = 0.5$, $G_c = 1$, $G_r = 1$, $S_c = 1.5$, $S = 1$, $\epsilon = 1$, $t = 2$, $\rho = 0.8$, $P = 1$, $\mu = 1$, $E = 0.5$, $w_0 = 3$, and $K_c = 1$, except where they are treated as variables.

The influence of various flow parameters on the velocity distribution $q(z,t)$ is illustrated in 2 to 7. Figure 2a shows that an increase in the rotation parameter E enhances the velocity in the vicinity of the plate, indicating that system rotation promotes fluid acceleration. As depicted in Figure 2b, the velocity magnitude increases significantly with an increase in the small positive constant ε, highlighting its strengthening effect on the flow field.

Figure 2c demonstrates that the velocity increases with increasing mass Grashof number G_c, which can be attributed to the intensification of buoyancy forces arising from concentration gradients. Likewise, Figure 2d reveals that higher values of the thermal Grashof number G_r lead to an enhancement of the velocity profile due to stronger thermal buoyancy effects.

Figure 3a illustrates that an increase in the porosity parameter K results in higher velocity, implying that increased permeability of the porous medium reduces flow resistance. In contrast, Figure 3b indicates that increasing the magnetic parameter M suppresses the velocity because of the Lorentz force, which acts against the motion of the electrically conducting fluid.

Figure 3c shows that the velocity slightly decreases with an increase in viscosity μ, reflecting the retarding influence of viscous forces. Finally, Figure 3d demonstrates that the velocity decreases with increasing oscillation frequency ω, confirming that higher oscillatory frequencies exert a damping effect on the fluid motion. Figure 4a shows that the fluid velocity increases with an increase in the pressure gradient parameter P. Figure 4b indicates that higher values of the couple-stress parameter (ϕ) suppress the velocity field. As illustrated in Figure 4c, the velocity decreases with an increase in the Prandtl number P_r, which is attributed to the reduction in thermal diffusivity. Figure 4d demonstrates that an increase in the density parameter (ρ) leads to a slight reduction in velocity.

Figs. 5(a)–5(c) illustrate the effect of the heat source parameter S on the velocity distribution. It is observed that positive values of S, corresponding to heat generation, enhance the velocity, whereas negative values of S, representing heat absorption, reduce the velocity field. Figure 5d reveals that the Schmidt number S_c has a negligible influence on the velocity.

Figure 6a indicates that the velocity decreases with the progression of time. Figure 6b shows that increasing the constant suction velocity parameter w_0 results in a reduction of velocity due to the thinning of the momentum boundary layer. Furthermore, Figs. 7(a)–7(c) demonstrate that the chemical reaction parameter K_c has a significant effect on the velocity field; positive values of K_c decrease the velocity, while negative values lead to an enhancement of velocity.

Figures 8 and 9 present the effects of various flow parameters on the temperature distribution $T(z,t)$. Figure 8a illustrates the influence of the small positive constant ε on the temperature profile. It is observed that an increase in ε leads to a significant enhancement in temperature, indicating an increase in thermal energy within the boundary layer. This effect is more pronounced in the vicinity of the plate and gradually diminishes as the distance from the plate increases.

Figure 8b depicts the impact of the oscillation frequency ω on temperature. The results indicate that an increase in ω results in a decrease in temperature. Physically, higher oscillation frequencies intensify

thermal disturbances, which enhances heat dissipation and consequently reduces the thickness of the thermal boundary layer.The effect of the Prandtl number P_r on the temperature distribution is shown in Figure 8c. It is evident that temperature decreases with increasing P_r. This behavior can be attributed to the lower thermal diffusivity compared to momentum diffusivity at higher Prandtl numbers, leading to a thinner thermal boundary layer.

Figure 8d illustrates the influence of the negative heat source parameter $(S < 0)$ on the temperature profile. An increase in the magnitude of the negative heat source parameter results in a noticeable reduction in temperature, indicating the predominance of heat absorption within the fluid.Figure 9a demonstrates the effect of the positive heat source parameter $(S > 0)$. It is observed that increasing S enhances the temperature due to internal heat generation, which causes an increase in the thermal boundary layer thickness. Figure 9b compares the temperature profiles for both positive and negative values of the heat source parameter. Positive values of S lead to an increase in temperature, whereas negative values cause a reduction, confirming the opposing effects of heat generation and heat absorption mechanisms. Finally, Figure 9c shows the variation of temperature with respect to time (t). The temperature initially increases with time near the plate and subsequently exhibits a gradual decay along the transverse direction. This behavior reflects the combined influence of transient effects and oscillatory flow dynamics.

Figures 10 illustrate the influence of various flow parameters on the concentration distribution $C(z,t)$. Figure 10a shows that increasing the mass transfer constant ε reduces the concentration, indicating that stronger mass transfer effects suppress the concentration field. The effect of oscillation frequency ω is depicted in Figure 10b, where higher values of ω enhance the concentration due to intensified oscillatory motion of the fluid. Figure 10c presents the impact of the Schmidt number S_c, demonstrating that an increase in S_c leads to a decrease in concentration as a result of reduced mass diffusivity and a thinner concentration boundary layer. The temporal evolution of concentration is shown in Figure 10d, revealing an increase in concentration with time t as diffusion becomes more pronounced. Figures 11 illustrate the effect of the chemical reaction parameter K_c on the concentration distribution.

Figure 11a indicates that for positive values of K_c (destructive reaction), increasing K_c causes a reduction in concentration due to enhanced consumption of the diffusing species. Conversely, Figure 11b demonstrates that for negative values of K_c (generative reaction), an increase in the magnitude of K_c enhances the concentration profile.

Moreover, Figure 11c shows that the concentration boundary layer thickness is significantly influenced by K_c, with stronger generative reactions leading to higher concentration levels.The numerical variations of the shear stress (τ), Nusselt number (N_u), and Sherwood number (S_h) with respect to various governing flow parameters are summarized in Tables 1–18. Table 1 demonstrates that the shear stress at the plate decreases with an increase in the magnetic parameter (Hartmann number M) from 0 to 4 for all phase angles, owing to the resistive Lorentz force that opposes the fluid motion.

According to Table 2, the shear stress increases as the couple-stress parameter ϕ decreases from 10 to

6, indicating that weaker couple-stress effects intensify fluid motion in the vicinity of the plate. Table 3 shows that an increase in the porosity parameter K from 0.2 to 0.6 leads to higher shear stress, since greater permeability reduces the resistance to flow. Table 4 reveals a non-monotonic variation of shear stress with the Prandtl number P_r, reflecting the non-uniform role of thermal diffusivity. From Table 5, it is observed that an increase in the mass Grashof number G_c from 2 to 15 causes a reduction in shear stress for $\omega t = 0, \pi/4$, and $\pi/2$ and , whereas an opposite trend is noted at $\omega t = 3\pi/4$. Table 6 indicates a pronounced increase in shear stress with increasing thermal Grashof number G_r from 1 to 5, highlighting the strengthening influence of thermal buoyancy on the velocity field.

Table 7 shows a slight increase in shear stress with rising Schmidt number S_c, signifying the effect of mass diffusivity. Table 8 illustrates that shear stress exhibits a marginal increase with suction velocity w_0 at $\omega t = 0, \pi/4$, and $\pi/2$, while a decreasing tendency is observed at $\omega t = 3\pi/4$. Table 9 suggests that variations in fluid density ρ have a negligible effect on shear stress. As seen in Table 10, shear stress slightly decreases with an increase in the pressure gradient parameter P from 1 to 5 for $\omega t = 0, \pi/4$, and $\pi/2$, whereas a mild increase is recorded at $\omega t = 3\pi/4$. Table 11 shows that increasing viscosity μ from 1 to 5 results in a gradual reduction in shear stress for $\omega t = 0, \pi/4$, and $\pi/2$, while a small enhancement occurs at $\omega t = 3\pi/4$, indicating the suppressive effect of viscous resistance on velocity gradients.

Table 12 reveals a continuous decrease in shear stress with increasing rotation parameter E from 0.1 to 1.5 for all phase angles, implying that stronger rotation retards fluid motion. Table 13 indicates a mixed response of shear stress to the heat source parameter S, depending on the phase angle. Table 14 shows that shear stress decreases slightly as the chemical reaction parameter K_c increases from -0.2 to 0.2. With regard to heat transfer, Table 15 indicates that the Nusselt number increases as the Prandtl number P_r rises from 0.7 to 3 and then decreases at higher values, suggesting optimal heat transfer at moderate Prandtl numbers.

Table 16 demonstrates that the Nusselt number decreases with increasing heat source parameter S for all phase angles, confirming that internal heat generation diminishes the heat transfer rate at the plate. Table 17 shows that the Sherwood number increases monotonically with the Schmidt number S_c, indicating an enhancement in mass transfer.

Finally, Table 18 reveals that the Sherwood number increases with increasing chemical reaction parameter K_c from -0.2 to 0.2 for all phase angles, implying that stronger chemical reactions promote mass transfer.

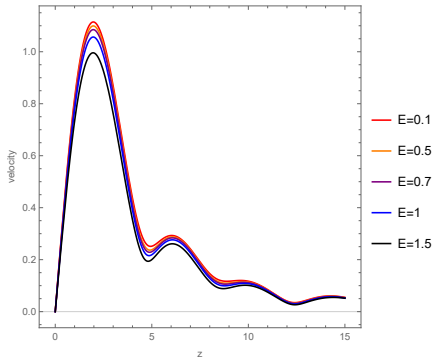

(a) Variation of $q(z,t)$ for (Rotation parameter E).

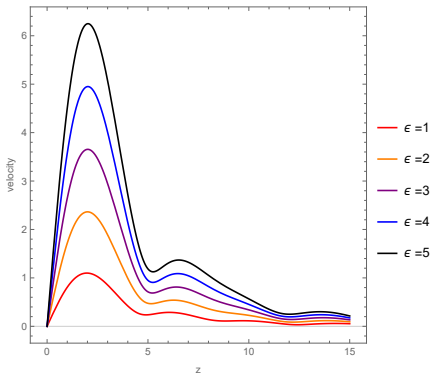

(b) Variation of $q(z,t)$ for (A small positive constant ϵ).

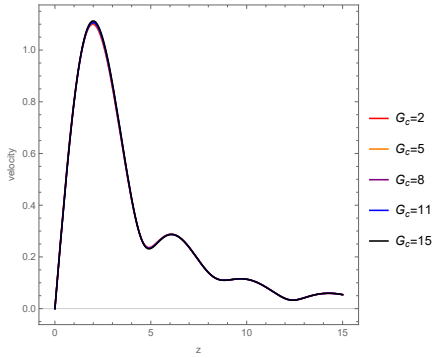

(c) Variation of $q(z,t)$ for (Mass Grashof number G_c).

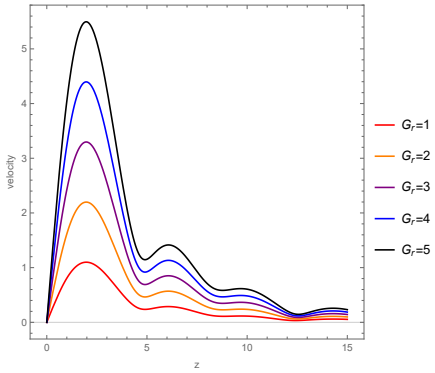

(d) Variation of $q(z,t)$ for (Thermal Grashof number G_r).

Figure 2: Variation of velocity with different flow parameters

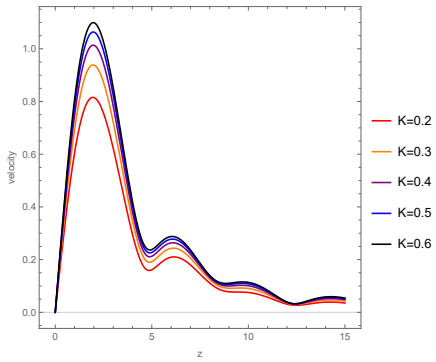

(a) Variation of $q(z,t)$ for (Porosity parameter K).

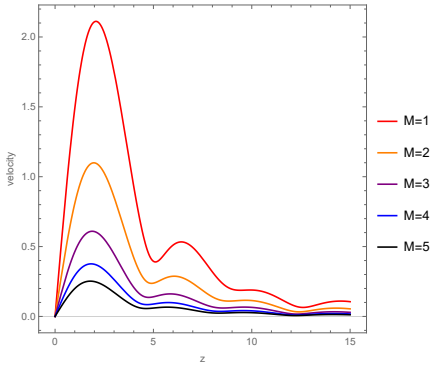

(b) Variation of $q(z,t)$ for (Magnetic parameter M).

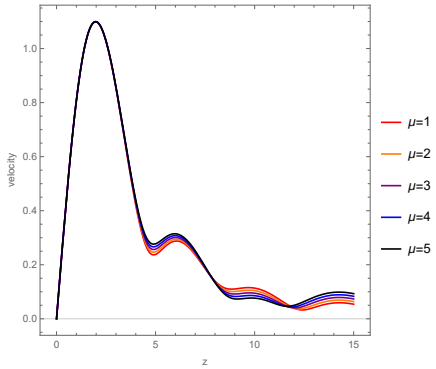

(c) Variation of $q(z,t)$ for (Viscosity μ).

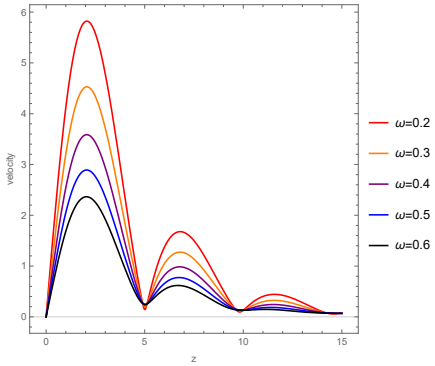

(d) Variation of $q(z,t)$ for (Frequency of oscillation ω).

Figure 3: Variation of velocity with different flow parameters

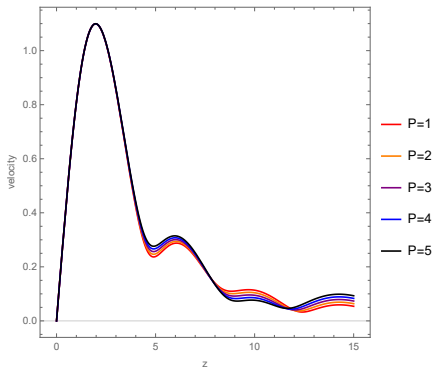

(a) Variation of $q(z,t)$ for (Pressure gradient P).

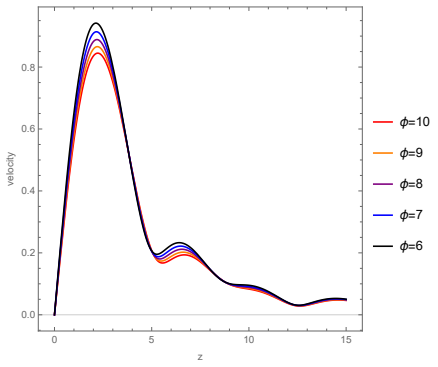

(b) Variation of $q(z,t)$ for (Couple Stress parameter ϕ).

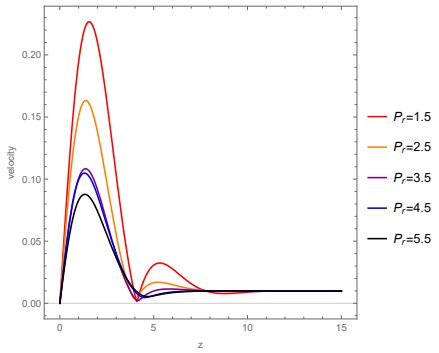

(c) Variation of $q(z,t)$ for (Prandtl number P_r).

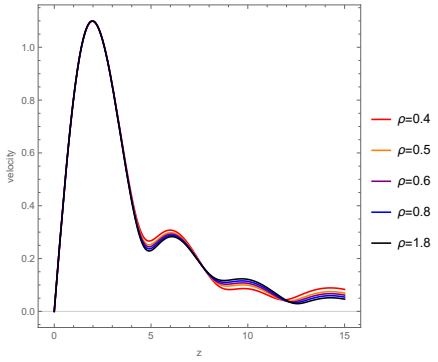

(d) Variation of $q(z,t)$ for (Density of the fluid ρ).

Figure 4: Variation of velocity with different flow parameters

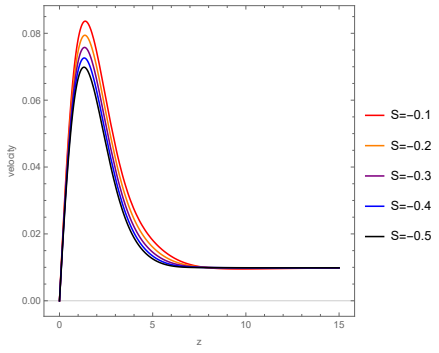

(a) Variation of $q(z,t)$ for (Heat source parameter S).

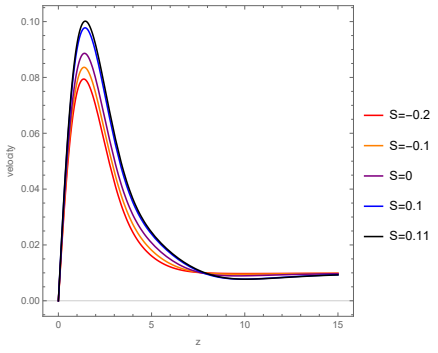

(b) Variation of $q(z,t)$ for (Heat source parameter S).

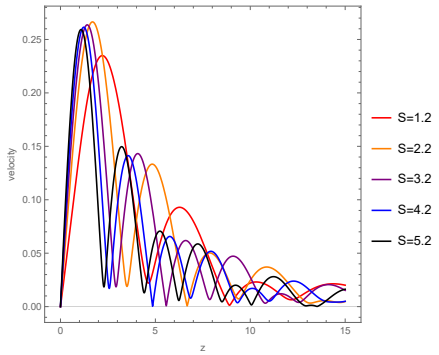

(c) Variation of $q(z,t)$ for (Heat source parameter S).

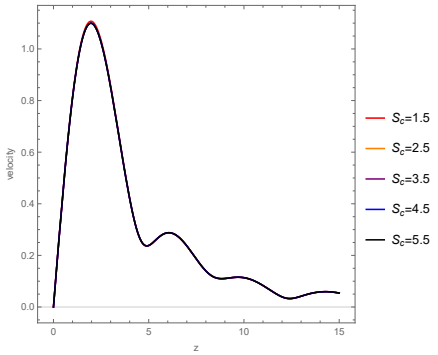

(d) Variation of $q(z,t)$ for (Schmidt number S_c).

Figure 5: Variation of velocity with different flow parameters

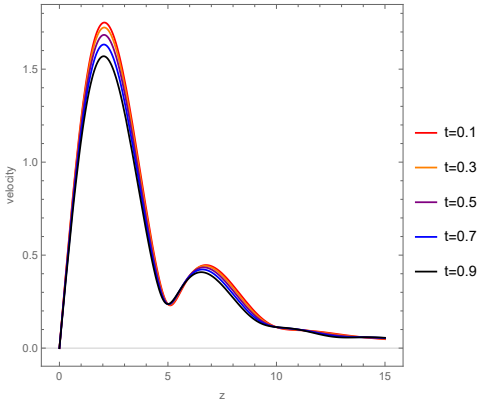

(a) Variation of $q(z,t)$ for (Time t).

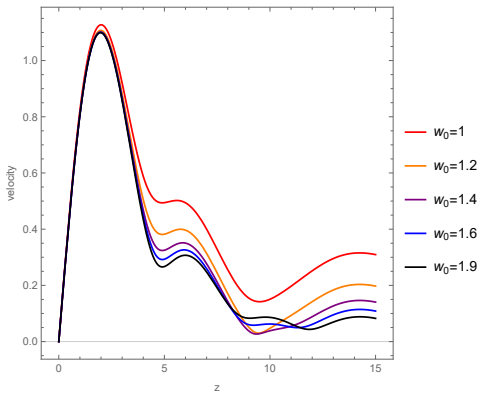

(b) Variation of $q(z,t)$ for (Constant suction velocity w_0).

Figure 6: Variation of velocity with different flow parameters

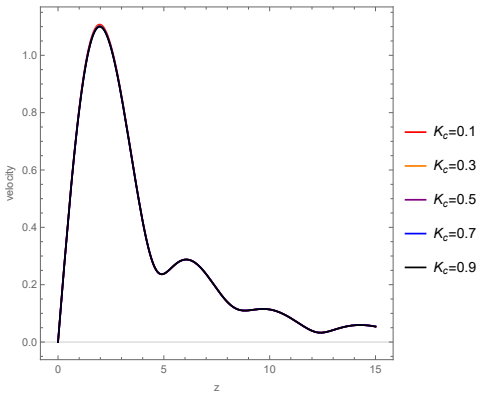

(a) Variation of $q(z,t)$ for (Chemical rection parameter K_c) .

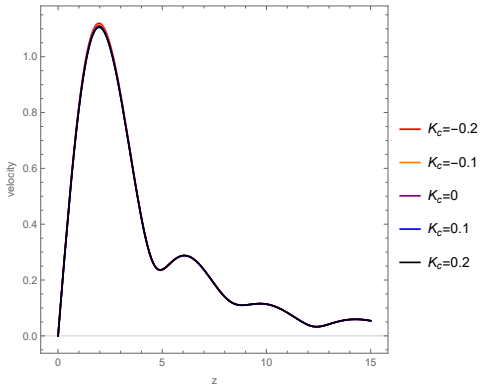

(b) Variation of $q(z,t)$ for (Chemical rection parameter K_c) .

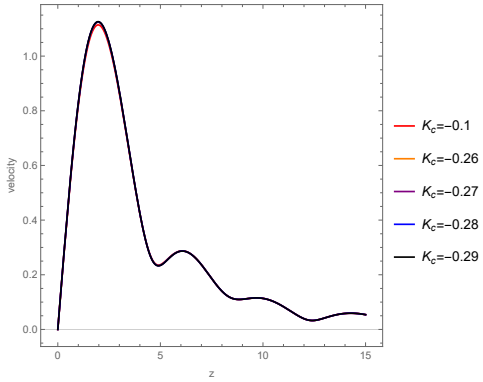

(c) Variation of $q(z,t)$ for (Chemical rection parameter K_c) .

Figure 7: Variation of velocity with different flow parameters

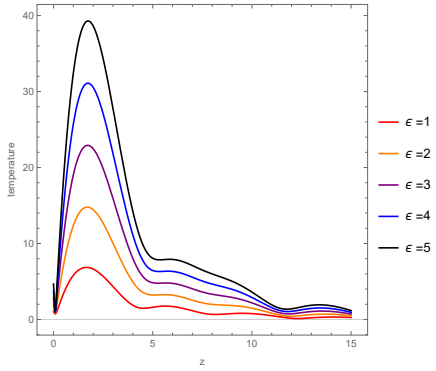

(a) Variation of $T(z,t)$ for (A small positive constant ϵ).

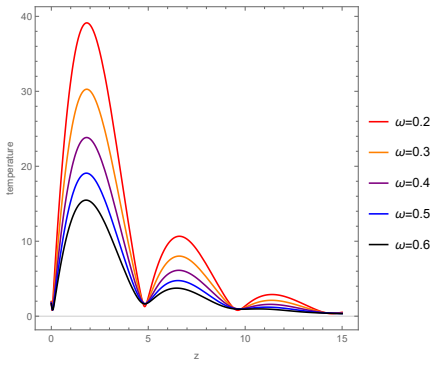

(b) Variation of $T(z,t)$ for (Oscillation frequency ω).

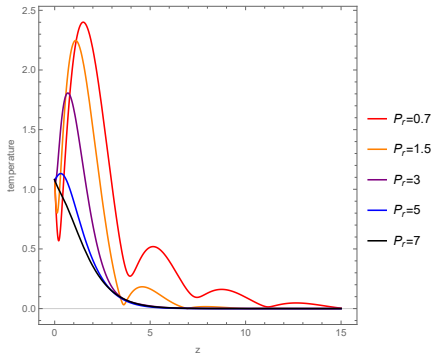

(c) Variation of $T(z,t)$ for (Prandtl number P_r).

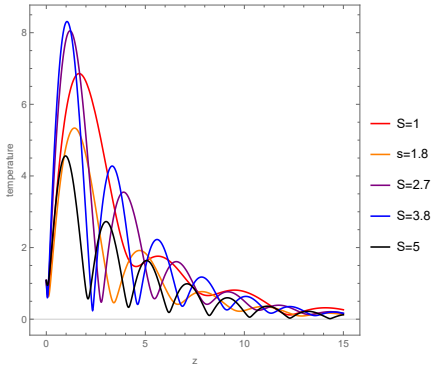

(d) Variation of $T(z,t)$ for (Heat source parameter S).

Figure 8: Variation of temperature with different flow parameters

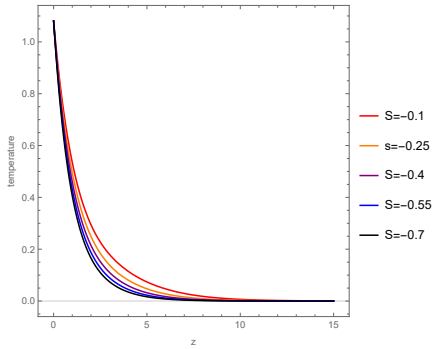

(a) Variation of $T(z,t)$ for (Heat source parameter S).

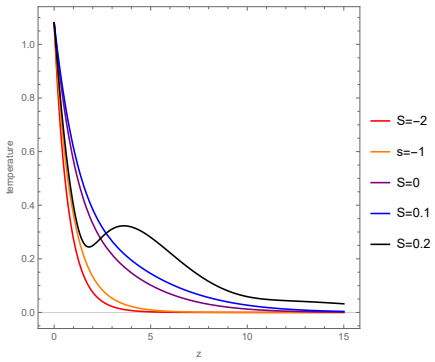

(b) Variation of $T(z,t)$ for (Heat source parameter S).

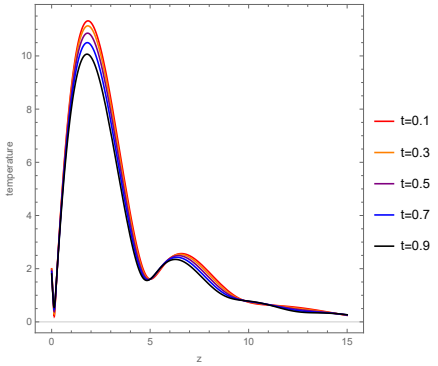

(c) Variation of $T(z,t)$ for (Time t).

Figure 9: Variation of temperature with different flow parameters

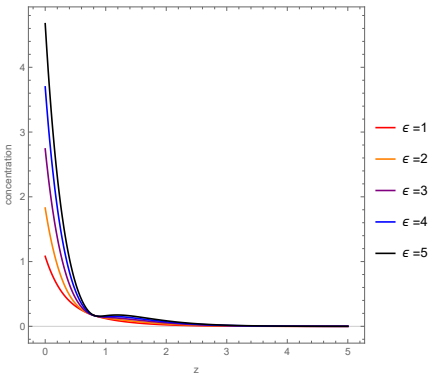

(a) Variation of $C(z,t)$ for (A small positive constant ϵ).

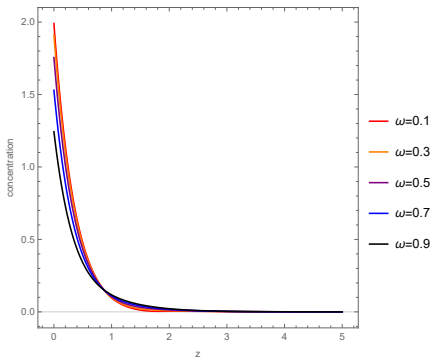

(b) Variation of $C(z,t)$ for (Oscillation frequency ω).

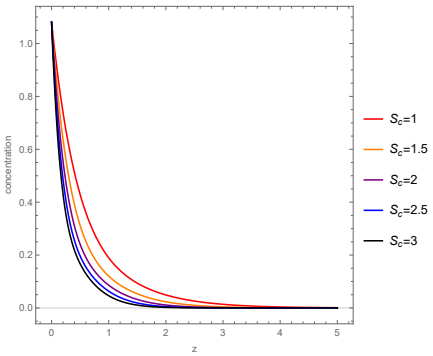

(c) Variation of $C(z,t)$ for (Schmidt number S_c).

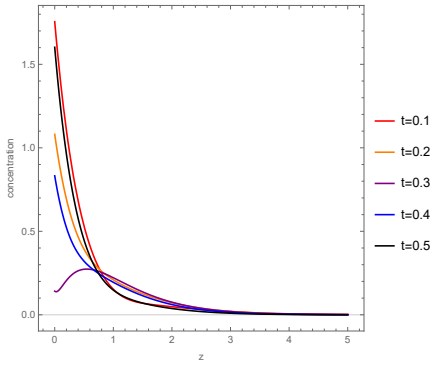

(d) Variation of $C(z,t)$ for (Time t).

Figure 10: Variation of concentration with different flow parameters

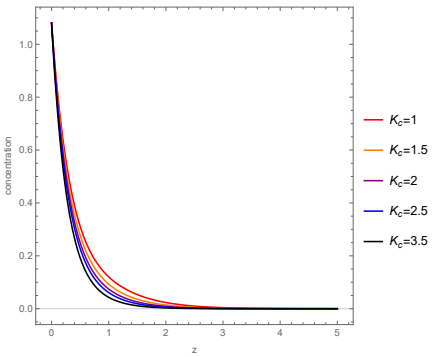

(a) Variation of $C(z,t)$ for (Chemical rection parameter K_c) .

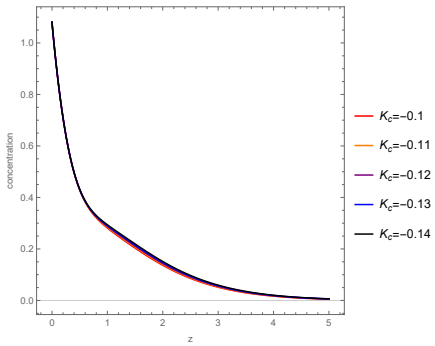

(b) Variation of $C(z,t)$ for (Chemical rection parameter K_c).

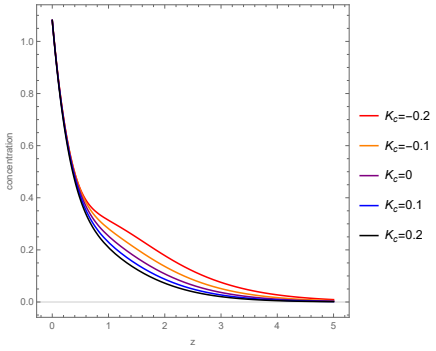

(c) Variation of $C(z,t)$ for (Chemical rection parameter K_c).

Figure 11: Variation of concentration with different flow parameters

ωt	$M = 0$	$M = 1$	$M = 2$	$M = 3$	$M = 4$
0	52.4365	39.9564	23.4595	14.1031	9.14829
$\frac{\pi}{4}$	6.7469	5.06817	2.90152	1.71111	1.09457
$\frac{\pi}{2}$	3.2649	2.41043	1.34647	0.783523	0.497927
$\frac{3\pi}{4}$	1.66434	1.20164	0.65232	0.377504	0.241524

Table 1: Variation in Share Stress at the Plate with Magnetic Parameter M at $\omega = 1$, $\phi = 2$, $K = 0.6$, $P_r = 0.5$, $G_c = 1$, $G_r = 1$, $S_c = 1.5$, $S = 1$, $\epsilon = 1$, $t = 2$, $\rho = 0.8$, $P = 1$, $\mu = 1$, $E = 0.5$, $w_0 = 3$, $K_c = 1$.

ωt	$\phi = 10$	$\phi = 9$	$\phi = 8$	$\phi = 7$	$\phi = 6$
0	16.6963	17.2127	17.7818	18.4147	19.1266
$\frac{\pi}{4}$	2.06414	2.12812	2.19869	2.27722	2.36562
$\frac{\pi}{2}$	0.939318	0.96984	1.00362	1.04137	1.08405
$\frac{3\pi}{4}$	0.428873	0.444631	0.462244	0.482141	0.50492

Table 2: Variation in Share Stress at the Plate with Couple Stress Parameter ϕ at $M = 2$, $\omega = 1$, $K = 0.6$, $P_r = 0.5$, $G_c = 1$, $G_r = 1$, $S_c = 1.5$, $S = 1$, $\epsilon = 1$, $t = 2$, $\rho = 0.8$, $P = 1$, $\mu = 1$, $E = 0.5$, $w_0 = 3$, $K_c = 1$.

ωt	$K = 0.2$	$K = 0.3$	$K = 0.4$	$K = 0.5$	$K = 0.6$
0	16.3087	19.2196	21.1216	22.4627	23.4595
$\frac{\pi}{4}$	2.05006	2.40191	2.62797	2.78549	2.90152
$\frac{\pi}{2}$	0.981123	1.13612	1.2328	1.29871	1.34647
$\frac{3\pi}{4}$	0.509843	0.574762	0.612099	0.635946	0.65232

Table 3: Variation in Share Stress at the Plate with Porosity Parameter K at $M = 2$, $\omega = 1$, $\phi = 2$, $P_r = 0.5$, $G_c = 1$, $G_r = 1$, $S_c = 1.5$, $S = 1$, $\epsilon = 1$, $t = 2$, $\rho = 0.8$, $P = 1$, $\mu = 1$, $E = 0.5$, $w_0 = 3$, $K_c = 1$.

ωt	$P_r = 1.5$	$P_r = 2.5$	$P_r = 3.5$	$P_r = 4.5$	$P_r = 5.5$
0	8.81718	67.8055	20.6515	0.244198	0.218506
$\frac{\pi}{4}$	0.962098	1.63917	0.390857	0.226272	0.201968
$\frac{\pi}{2}$	0.368527	0.274282	0.663495	0.17763	0.154636
$\frac{3\pi}{4}$	0.182313	0.233993	0.179997	0.116196	0.0916394

Table 4: Variation in Share Stress at the Plate with Prandtl number P_r at $M = 2$, $\omega = 1$, $\phi = 2$, $K = 0.6$, $G_c = 1$, $G_r = 1$, $S_c = 1.5$, $S = 1$, $\epsilon = 1$, $t = 2$, $\rho = 0.8$, $P = 1$, $\mu = 1$, $E = 0.5$, $w_0 = 3$, $K_c = 1$.

ωt	$G_c = 2$	$G_c = 5$	$G_c = 8$	$G_c = 11$	$G_c = 15$
0	23.4254	23.323	23.2206	23.1182	22.9817
$\frac{\pi}{4}$	2.87477	2.7952	2.71672	2.63942	2.5384
$\frac{\pi}{2}$	1.33223	1.29177	1.25497	1.22215	1.18515
$\frac{3\pi}{4}$	0.653999	0.662083	0.674599	0.691307	0.719587

Table 5: Variation in Share Stress at the Plate with Mass Grashof number G_c at $M = 2$, $\omega = 1$, $\phi = 2$, $K = 0.6$, $P_r = 0.5$, $G_r = 1$, $S_c = 1.5$, $S = 1$, $\epsilon = 1$, $t = 2$, $\rho = 0.8$, $P = 1$, $\mu = 1$, $E = 0.5$, $w_0 = 3$, $K_c = 1$.

ωt	$G_r = 1$	$G_r = 2$	$G_r = 3$	$G_r = 4$	$G_r = 5$
0	23.4595	46.9649	70.4703	93.9758	117.481
$\frac{\pi}{4}$	2.90152	5.83828	8.77509	11.7119	14.6487
$\frac{\pi}{2}$	1.34647	2.71103	4.07571	5.44042	6.80514
$\frac{3\pi}{4}$	0.65232	1.30091	1.94968	2.59849	3.24732

Table 6: Variation in Share Stress at the Plate with Thermal Grashof number G_r at $M = 2$, $\omega = 1$, $\phi = 2$, $K = 0.6$, $P_r = 0.5$, $G_c = 1$, $S_c = 1.5$, $S = 1$, $\epsilon = 1$, $t = 2$, $\rho = 0.8$, $P = 1$, $\mu = 1$, $E = 0.5$, $w_0 = 3$, $K_c = 1$.

ωt	$S_c = 1.5$	$S_c = 2.5$	$S_c = 3.5$	$S_c = 4.5$	$S_c = 5.5$
0	23.4595	23.4776	23.4848	23.4882	23.49
$\frac{\pi}{4}$	2.90152	2.91645	2.92213	2.92475	2.92613
$\frac{\pi}{2}$	1.34647	1.35606	1.3593	1.36058	1.36114
$\frac{3\pi}{4}$	0.65232	0.6551	0.65519	0.654752	0.654255

Table 7: Variation in Shear Stress at the Plate with Schmidt number S_c at $M = 2$, $\omega = 1$, $\phi = 2$, $K = 0.6$, $P_r = 0.5$, $G_c = 1$, $G_r = 1$, $S = 1$, $\epsilon = 1$, $t = 2$, $\rho = 0.8$, $P = 1$, $\mu = 1$, $E = 0.5$, $w_0 = 3$, $K_c = 1$.

ωt	$w_0 = 1$	$w_0 = 1.2$	$w_0 = 1.4$	$w_0 = 1.6$	$w_0 = 1.9$
0	23.1523	23.2867	23.3551	23.3934	23.4248
$\frac{\pi}{4}$	2.90152	2.89984	2.89816	2.89649	2.89398
$\frac{\pi}{2}$	1.27949	1.30276	1.31826	1.328	1.33651
$\frac{3\pi}{4}$	0.746751	0.699107	0.678476	0.66808	0.660249

Table 8: Variation in Share Stress at the Plate with Constant Suction velocity w_0 at $M = 2$, $\omega = 1$, $\phi = 2$, $K = 0.6$, $P_r = 0.5$, $G_c = 1$, $G_r = 1$, $S_c = 1.5$, $S = 1$, $\epsilon = 1$, $t = 2$, $\rho = 0.8$, $P = 1$, $\mu = 1$, $E = 0.5$, $K_c = 1$.

Table 9: Variation in Share Stress at the Plate with Density of the Fluid ρ at $M = 2$, $\omega = 1$, $\phi = 2$, $K = 0.6$, $P_r = 0.5$, $G_c = 1$, $G_r = 1$, $S_c = 1.5$, $S = 1$, $\epsilon = 1$, $t = 2$, $P = 1$, $\mu = 1$, $E = 0.5$, $w_0 = 3$, $K_c = 1$.

ωt	$\rho = 0.4$	$\rho = 0.5$	$\rho = 0.6$	$\rho = 0.8$	$\rho = 1.8$
0	23.424	23.4411	23.4503	23.4595	23.469
$\frac{\pi}{4}$	2.87645	2.88846	2.895	2.90152	2.90826
$\frac{\pi}{2}$	1.3363	1.3411	1.34377	1.34647	1.34929
$\frac{3\pi}{4}$	0.660429	0.656435	0.654344	0.65232	0.650289

ωt	$P=1$	$P=2$	$P=3$	$P=4$	$P=5$
0	23.4595	23.4477	23.4359	23.424	23.4122
$\frac{\pi}{4}$	2.90152	2.89314	2.88478	2.87645	2.86813
$\frac{\pi}{2}$	1.34647	1.34301	1.33962	1.3363	1.33304
$\frac{3\pi}{4}$	0.65232	0.654932	0.657636	0.660429	0.663312

Table 10: Variation in Share Stress at the Plate with Pressure gradient P at $M=2$, $\omega=1$, $\phi=2$, $K=0.6$, $P_r=0.5$, $G_c=1$, $G_r=1$, $S_c=1.5$, $S=1$, $\epsilon=1$, $t=2$, $\rho=0.8$, $\mu=1$, $E=0.5$, $w_0=3$, $K_c=1$.

ωt	$\mu=1$	$\mu=2$	$\mu=3$	$\mu=4$	$\mu=5$
0	23.4595	23.4477	23.4359	23.4240	23.4122
$\frac{\pi}{4}$	2.90152	2.89314	2.88478	2.87645	2.86813
$\frac{\pi}{2}$	1.34647	1.34301	1.33962	1.3363	1.33304
$\frac{3\pi}{4}$	0.65232	0.654932	0.657636	0.660429	0.663312

Table 11: Variation in Share Stress at the Plate with Viscosity μ at $M=2$, $\omega=1$, $\phi=2$, $K=0.6$, $P_r=0.5$, $G_c=1$, $G_r=1$, $S_c=1.5$, $S=1$, $\epsilon=1$, $t=2$, $\rho=0.8$, $P=1$, $E=0.5$, $w_0=3$, $K_c=1$.

ωt	$E=0.1$	$E=0.5$	$E=0.7$	$E=1$	$E=1.5$
0	23.6965	23.4595	23.2303	22.7672	21.7511
$\frac{\pi}{4}$	2.93948	2.90152	2.86808	2.80266	2.66333
$\frac{\pi}{2}$	1.36798	1.34647	1.32859	1.29439	1.22315
$\frac{3\pi}{4}$	0.664418	0.65232	0.642508	0.623961	0.585951

Table 12: Variation in Share Stress at the Plate with Rotation Parameter E at $M=2$, $\omega=1$, $\phi=2$, $K=0.6$, $P_r=0.5$, $G_c=1$, $G_r=1$, $S_c=1.5$, $S=1$, $\epsilon=1$, $t=2$, $\rho=0.8$, $P=1$, $\mu=1$, $w_0=3$, $K_c=1$.

ωt	$S = -0.2$	$S = -0.1$	$S = 0$	$S = 0.1$	$S = 0.11$
0	0.182716	0.189591	0.196832	0.187462	0.173295
$\frac{\pi}{4}$	0.170783	0.177272	0.184617	0.195751	0.199143
$\frac{\pi}{2}$	0.135829	0.141074	0.147345	0.158858	0.161782
$\frac{3\pi}{4}$	0.0846332	0.0880587	0.0920882	0.0990498	0.100716

Table 13: Variation in Share Stress at the Plate with Heat Source Parameter S at $M = 2$, $\omega = 1$, $\phi = 2$, $K = 0.6$, $P_r = 0.5$, $G_c = 1$, $G_r = 1$, $S_c = 1.5$, $\epsilon = 1$, $t = 2$, $\rho = 0.8$, $P = 1$, $\mu = 1$, $E = 0.5$, $w_0 = 3$, $K_c = 1$.

ωt	$K_c = -0.2$	$K_c = -0.1$	$K_c = 0$	$K_c = 0.1$	$K_c = 0.2$
0	23.4616	23.456	23.4542	23.4539	23.4541
$\frac{\pi}{4}$	2.90708	2.9023	2.90017	2.89924	2.89893
$\frac{\pi}{2}$	1.35963	1.35486	1.3518	1.34984	1.34858
$\frac{3\pi}{4}$	0.675612	0.669996	0.665759	0.662599	0.660209

Table 14: Variation in Share Stress at the Plate with Chemical rection parameter K_c at $M = 2$, $\omega = 1$, $\phi = 2$, $K = 0.6$, $P_r = 0.5$, $G_c = 1$, $G_r = 1$, $S_c = 1.5$, $S = 1$, $\epsilon = 1$, $t = 2$, $\rho = 0.8$, $P = 1$, $\mu = 1$, $E = 0.5$, $w_0 = 3$.

ωt	$P_r = 0.7$	$P_r = 1.5$	$P_r = 3$	$P_r = 5$	$P_r = 7$
0	42.0255	196.46	836.85	0.189419	0.571102
$\frac{\pi}{4}$	4.8035	6.31277	6.10299	2.41096	1.754
$\frac{\pi}{2}$	6.59861	8.78004	38.0014	2.04	1.52889
$\frac{3\pi}{4}$	3.65174	5.0646	5.42254	2.63232	1.87485

Table 15: Variation in Nusslet Number at the Plate with Prandtl Number P_r at $M = 2$, $\omega = 1$, $\phi = 2$, $K = 0.6$, $G_c = 1$, $G_r = 1$, $S_c = 1.5$, $S = 1$, $\epsilon = 1$, $t = 2$, $\rho = 0.8$, $P = 1$, $\mu = 1$, $E = 0.5$, $w_0 = 3$, $K_c = 1$.

ωt	$S = 1$	$S = 1.8$	$S = 2.7$	$S = 3.8$	$S = 5$
0	225.395	44.3635	54.0647	37.0157	7.95094
$\frac{\pi}{4}$	9.90038	8.57231	14.0665	16.0834	9.18002
$\frac{\pi}{2}$	14.3763	11.8142	18.9712	21.0711	11.744
$\frac{3\pi}{4}$	7.06834	6.50078	10.9101	12.774	7.63199

Table 16: Variation in Nusslet Number at the Plate with Heat Source Parameter S at $M = 2$, $\omega = 1$, $\phi = 2$, $K = 0.6$, $P_r = 0.5$, $G_c = 1$, $G_r = 1$, $S_c = 1.5$, $\epsilon = 1$, $t = 2$, $\rho = 0.8$, $P = 1$, $\mu = 1$, $E = 0.5$, $w_0 = 3$, $K_c = 1$.

ωt	$S_c = 1$	$S_c = 1.5$	$S_c = 2$	$S_c = 2.5$	$S_c = 3$
0	3.95967	5.51396	7.04145	8.55635	10.0646
$\frac{\pi}{4}$	3.65987	5.10386	6.52441	7.93417	9.33834
$\frac{\pi}{2}$	2.81398	3.94871	5.06993	6.18577	7.29933
$\frac{3\pi}{4}$	2.17668	3.08187	3.98181	4.88093	5.78063

Table 17: Variation in Sherwood Number at the Plate with Schmidt Number S_c at $M = 2$, $\omega = 1$, $\phi = 2$, $K = 0.6$, $P_r = 0.5$, $G_c = 1$, $G_r = 1$, $S = 1$, $\epsilon = 1$, $t = 2$, $\rho = 0.8$, $P = 1$, $\mu = 1$, $E = 0.5$, $w_0 = 3$, $K_c = 1$.

ωt	$K_c = -0.2$	$K_c = -0.1$	$K_c = 0$	$K_c = 0.1$	$K_c = 0.2$
0	4.37258	4.41033	4.5	4.60459	4.7131
$\frac{\pi}{4}$	4.0793	4.11406	4.19061	4.2818	4.37785
$\frac{\pi}{2}$	3.2864	3.29396	3.33025	3.38192	3.44136
$\frac{3\pi}{4}$	2.72146	2.69918	2.70216	2.72178	2.75149

Table 18: Variation in Sherwood Number at the Plate with Chemical rection parameter K_c at $M = 2$, $\omega = 1$, $\phi = 2$, $K = 0.6$, $P_r = 0.5$, $G_c = 1$, $G_r = 1$, $S_c = 1.5$, $S = 1$, $\epsilon = 1$, $t = 2$, $\rho = 0.8$, $P = 1$, $\mu = 1$, $E = 0.5$, $w_0 = 3$.

6. Conclusion

The present investigation yields several physically significant observations concerning the velocity, temperature, and concentration distributions of the flow field, along with the associated skin friction, Nusselt number, and Sherwood number. The principal findings can be summarized as follows:
The velocity of the couple-stress fluid is found to decrease with increasing Hartmann number M, oscillation frequency ω, couple-stress parameter ϕ, and positive chemical reaction parameter K_c. This reduction in velocity is attributed to resistive mechanisms such as the Lorentz force induced by the magnetic field, the influence of internal couple stresses, and the consumption of species due to destructive chemical reactions.

- In contrast, an increase in the Grashof number for heat transfer G_r, the permeability parameter K_p, and the oscillatory suction parameter ε leads to an enhancement of the velocity field. This behavior arises from stronger buoyancy forces and increased permeability of the porous medium, which collectively facilitate fluid motion.

- The Prandtl number P_r plays a crucial role in governing both velocity and temperature distributions. Higher values of P_r correspond to lower thermal diffusivity, resulting in a thinner thermal boundary layer and a reduction in heat transfer within the flow.

- An increase in the Schmidt number S_c causes a decrease in both concentration and velocity profiles. This effect is associated with reduced mass diffusivity, which leads to the formation of a thinner concentration boundary layer and consequently weaker species transport.

- The heat source parameter S exhibits a dual influence on the flow characteristics. Positive values of S, representing internal heat generation, enhance both temperature and velocity fields, whereas negative values of S, corresponding to a heat sink, suppress temperature and velocity throughout the boundary layer.

- Chemical reaction effects are also significant. Positive values of the chemical reaction parameter K_c (destructive reactions) reduce velocity and concentration by consuming the diffusing species, while negative values of K_c (generative reactions) promote an increase in both velocity and concentration distributions.

- The skin friction coefficient at the plate decreases with increasing M and K_c, reflecting the dominant resistive effects of the magnetic field and chemical reactions. Conversely, skin friction increases with higher values of K_p, G_r, and S_c, due to enhanced buoyancy and mass transfer effects.

- The Nusselt number N_u exhibits mixed behavior with respect to the Prandtl number P_r and the heat source parameter S. In general, N_u increases with increasing S under oscillatory flow

conditions, while it remains constant at $\omega t = 0$.

- Finally, the Sherwood number S_h increases with both the Schmidt number S_c and the chemical reaction parameter K_c, indicating enhanced mass transfer rates under conditions of stronger diffusivity effects and generative chemical reactions.

- Overall, these results provide valuable insights into the combined influence of magnetic, thermal, and chemical effects on couple-stress fluid flow through a porous medium under oscillatory conditions.

Acknowledgment

The author acknowledge this work is part of the research program for the award of ph.d. degree to the first author. The authors express their gratitude to the learned reviewers for their valuable comments and suggestions which improved the present work to a great extent.

References

[1] S. S. Das, A. Satapathy, J. K. Das and J. P. Panda, *Mass transfer effects on MHD flow and heat transfer past a vertical porous plate through a porous medium under oscillatory suction and heat source*, Int. J. Heat Mass Transfer, 52(25-26)(2009), 5962-5969.

[2] R. Bhargava, R. Sharma and O. A. Bég, *Oscillatory chemically-reacting MHD free convection heat and mass transfer in a porous medium with Soret and Dufour effects: finite element modeling*, Int. J. Appl. Math. Mech., 5(6)(2009), 15-37.

[3] J. G. Kumar and P. V. Satyanarayana, *Mass transfer effects on MHD unsteady free convective Walter's memory flow with constant suction and heat sink*, Int. J. Appl. Math. Mech., 7(19)(2011), 97-109.

[4] V. Ravikumar, M. C. Raju and G. S. S. Raju, *Heat and mass transfer effects on MHD flow of viscous fluid through non-homogeneous porous medium in presence of temperature dependent heat source*, Int. J. Contemp. Math. Sci., 7(32)(2012), 1597-1604.

[5] S. A. Hussaini, M. V. Ramana Murthy and A. Waheedullah, *MHD unsteady memory convective flow through porous medium with variable suction*, J. Appl. Fluid Mech., (2013).

[6] S. R. Mishra, G. C. Dash and M. Acharya, *Mass and heat transfer effect on MHD flow of a visco-elastic fluid through porous medium with oscillatory suction and heat source*, Int. J. Heat Mass Transfer, 57(2)(2013), 433-438.

[7] M. M. Rahman, M. S. Khan and M. R. Islam, *Numerical investigation on MHD fluid flow in the presence of chemical reaction with Soret and Dufour effects over a vertical plate in a rotating system*, J. Appl. Phys. Sci. Int., 4(2)(2014), 77-88.

[8] B. Mohanty, S. R. Mishra, and H. B. Pattnaik, *MHD flow of a viscoelastic fluid through non-homogeneous porous medium with oscillatory suction and heat source/sink*, Int. J. Math. Educ., 4(2014), 21-34.

[9] G. S. Seth, R. Sharma and B. Kumbhakar, *Heat and mass transfer effects on unsteady MHD natural convection flow of a chemically reactive and radiating fluid through a porous medium past a moving vertical plate with arbitrary ramped temperature*, J. Appl. Fluid Mech., 9(1)(2015), 103-117.

[10] N. Ali, S. U. Khan, M. Sajid and Z. Abbas, *MHD flow and heat transfer of couple stress fluid over an oscillatory stretching sheet with heat source/sink in porous medium*, Alexandria Eng. J., 55(2)(2016), 915-924.

[11] M. Umamaheswar, M. C. Raju, S. V. K. Varma and C. Sucharitha, *MHD double diffusive and chemically reactive fluid flow through a rotating porous plate*, Int. J. Res.-Granthaalayah, 5(7)(2017), 363-373.

[12] J. K. Singh, G. S. Seth and S. G. Begum, *Unsteady MHD natural convective flow of a rotating fluid over an infinite vertical plate due to oscillatory movement of the free-stream with Hall and ion-slip currents*, Diffusion Foundations, 11(2017), 146-161.

[13] D. Pal and S. Biswas, *Magnetohydrodynamic convective-radiative oscillatory flow of a chemically reactive micropolar fluid in a porous medium*, Propulsion Power Res., 7(2)(2018), 158-170.

[14] A. Emeka, A. C. Paul and N. Chinedu, *Free convection boundary layer flow of a rotating MHD fluid past a vertical porous medium with thermal radiation*, Int. J. Appl. Sci. Math. Theory, 5(2)(2019).

[15] M. V. Krishna and A. J. Chamkha, *MHD peristaltic rotating flow of a couple stress fluid through a porous medium with wall and slip effects*, Spec. Top. Rev. Porous Media, 10(3)(2019).

[16] M. Das and U. Das, *Unsteady MHD rotating and chemically reacting fluid flow over an oscillating vertical surface in a Darcian porous regime*, Front. Heat Mass Transfer, 17(2021).

[17] O. T. Bafakeeh, K. Raghunath, F. Ali, M. Khalid, E. S. M. Tag-ElDin, M. Oreijah, K. Guedri, N. B. Khedher and M. I. Khan, *Hall current and Soret effects on unsteady MHD rotating flow of second-grade fluid through porous media under the influences of thermal radiation and chemical reactions*, Catalysts, 12(10)(2022), 1233.

[18] M. Naveed, M. Imran and S. Gul, *Heat transfer analysis in hydromagnetic flow of couple stress fluid in presence of homogeneous and heterogeneous chemical reactions over a porous oscillatory stretchable sheet*, Adv. Mech. Eng., 15(2)(2023).

[19] R. Mahesh, U. S. Mahabaleshwar, P. N. V. Kumar, H. F. Öztop and N. Abu-Hamdeh, *Impact of radiation on the MHD couple stress hybrid nanofluid flow over a porous sheet with viscous dissipation*, Results Eng., 17(2023).

[20] P. K. Sharma, B. K. Sharma and A. Kumar, *Mathematical analysis of chemically reacting species and radiation effects on MHD free convective flow through a rotating porous medium*, Acta Mech. Automatica, 18(2)(2024).

[21] V. K. Verma and A. F. Ansari, *Darcy–Brinkman flow in an anisotropic rotating porous channel under the influence of magnetic field*, J. Porous Media, 27(6)(2024).

[22] V. K. Verma and A. F. Ansari, *Effect of magnetic field and slip conditions on flow in a rotating porous channel with viscous dissipation*, Heat Transfer, 54(2)(2025), 1562-1573.